International Journal of Scientific Advances
ISSN: 2708-7972
Volume: 7 | Issue: 6 | Nov – Dec 2026 Available Online: www.ijscia.com
DOI: 10.51542/ijscia.v7i6.39

Structural Design and Performance Analysis of a Biopharmaceutical Freeze-Dryer Chamber

Mingchao Rong

School of Transportation and Vehicle Engineering, Shandong University of Technology, 266 Xincun West Road, Zhangdian District, Zibo, Shandong 255000, China

*Corresponding author: Mingchao Rong; 17866791037@163.com

ABSTRACT

A compact biopharmaceutical freeze-dryer chamber was assessed using numerical fields and analytical section calculations. For the initial 10 mm configuration, the reported maximum von Mises stress was 288.1 MPa, approximately 4.1% above the adopted 276.7 MPa benchmark; maximum total deformation was 0.064835 mm. At a constant local bending moment, 11 and 12 mm strips reduced bending normal stress by 17.4% and 30.6%, respectively, while increasing mass per unit wall area by 10% and 20%. At a −70 °C coolant setting, shelf surface temperatures estimated from the contours were approximately −42 °C. These results support preliminary design assessment and identify a conditional strength shortfall. The thickness comparison describes local section behavior, while the temperature readings characterize local chamber cooling.

keywords: freeze-dryer chamber; structural design; finite element analysis; external pressure; temperature field

INTRODUCTION

Freeze-dryer chambers withstand external pressure and maintain low temperatures; their structural and thermal characteristics affect operation. Carfagna et al. studied heat-transfer coefficients and cycle design [1]. Piechnik et al. investigated freezing numerically and experimentally and jointly designed refrigeration and airflow systems [2,3]. Srisuma et al. analyzed radiation-induced heat-transfer differences [4]. Zadravec et al. coupled equipment- and vial-scale models to predict spatial conditions and primary drying [5].

This study provides a preliminary structural and thermal assessment of a compact rounded rectangular chamber. Numerical fields describe the initial 10 mm configuration; 11 and 12 mm thicknesses are compared analytically using local wall strips. The analysis relates section properties to mass and identifies regions for structural and thermal refinement.

1 CHAMBER DESIGN AND ANALYSIS METHODS

1.1 Chamber Geometry

The chamber has external dimensions of 280 mm × 325 mm × 320 mm, 10 mm walls, 30 mm corner radii, a front frame, and external cooling channels (Figure 1). Four 260 mm × 300 mm shelves have a total geometric area of 0.312 m^2; usable area depends on edge clearances and product placement.

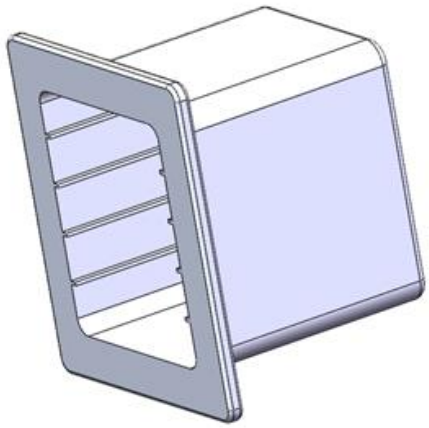


FIGURE 1: Three-dimensional model of the freeze-dryer chamber.

1.2 Materials and Modeling Assumptions

The structural model uses 2014-T6 aluminum: density 2793 kg/m^3, elastic modulus 72,398 MPa, Poisson's ratio 0.33, and nominal yield strength 415 MPa. Kaiser Aluminum's typical yield strength of 414 MPa for 2014-T6/T651 rod and bar [6] provides a comparison; low-temperature strength depends on product and temperature. With n_0 = 1.5, the preliminary strength benchmark is $\sigma_{ref} = \sigma_y/n_0$ = 276.667 MPa.

The thermal model uses Fluent's constant-property "aluminum" and "ethyl-siloxane-fluid" entries. Aluminum density, specific heat capacity, and thermal conductivity are 2719 kg/m^3, 871 J/(kg·K), and 202.4 W/(m·K); fluid values are 1050 kg/m^3, 1500 J/(kg·K), and 0.15 W/(m·K), with dynamic viscosity 0.001 Pa·s. The fluid represents a numerical medium; applications require properties matching the actual coolant and temperature.

1.3 Section Properties and Strength Assessment

A uniform rectangular strip of width b and thickness t represents the local wall. Equation (1) gives the second moment of area I, neutral-axis-to-surface distance c, and section modulus W [7]. Figure 2 shows the frame and loading locations; strip parameters are defined independently of the frame labels.

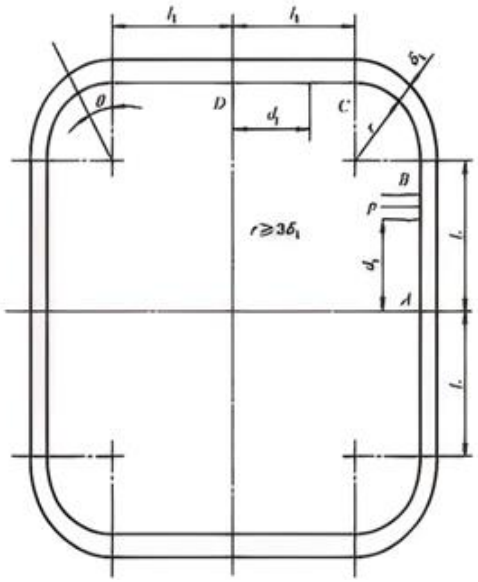


FIGURE 2: Rounded rectangular chamber frame and loading locations.

$$I = bt^3/12; \quad c = t/2; \quad W = I/c \quad (1)$$

For b = 1 mm and t = 10 mm, I = 83.333 mm^4, c = 5 mm, and W = 16.667 mm^3.

For a strip under axial force N and bending moment M, Eq. (2) gives the normal stresses on opposite surfaces and the governing stress [7]. The internal forces depend on loading, supports, and deformation compatibility.

$$\sigma_+ = N/(bt) + Mc/I; \quad \sigma_- = N/(bt) - Mc/I;$$

$$\sigma_{ctrl} = \max(|\sigma_+|, |\sigma_-|) \quad (2)$$

Equations (1) and (2) describe local linear elastic section behavior. The three-dimensional chamber is assessed using maximum von Mises stress and the strength indices in Eq. (3).

$$\sigma_{ref} = \sigma_y/n_0; \quad \eta = \sigma_{v,max}/\sigma_{ref}; \quad n_y = \sigma_y/\sigma_{v,max} \quad (3)$$

Here, σ_y is yield strength, $\sigma_{v,\,max}$ is maximum von Mises stress, η is stress utilization, and n_y is the yield-to-peak-stress ratio. The strength comparison criterion is $\eta \le 1$; sealing displacement and external-pressure stability require separate assessments.

1.4 Numerical Models and Loading Conditions

Geometry was created in SolidWorks, and structural analysis used ANSYS Workbench 2024 R1. Figure 3 shows the mesh; Table 1 summarizes mesh and loading parameters. The 5 mm minimum geometric edge length does not denote a uniform element size.

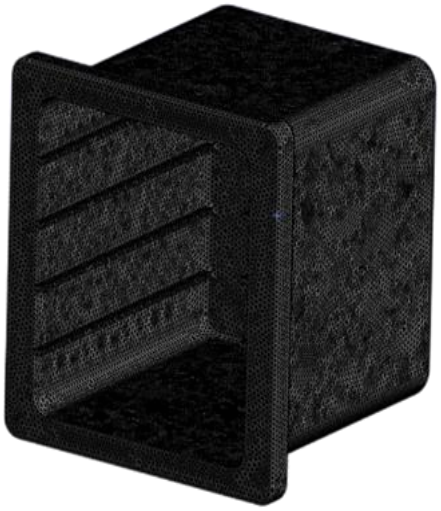


FIGURE 3: Structural finite element mesh of the chamber.

External pressure is 0.1 MPa. The associated steady-state thermal case specifies outer and inner temperatures of −55 °C and −20 °C. Figures 4 and 5 report structural responses; the available loading description does not establish their thermal contribution. The 1 s label denotes a static load step. The cooling case includes channels, chamber, and shelves, a −70 °C coolant setting, the energy equation, laminar flow, and radiation disabled.

TABLE 1: Mesh and loading parameters.

Model or case	Parameter	Value or setting
Structure	Nodes/elements	754132 / 492865
Structure	Mesh/geometry	Adaptive sizing; minimum geometric edge 5 mm
Structural case	External pressure	0.1 MPa
Associated thermal case	Outer/inner temperature	−55 °C / −20 °C
Cooling	Nodes/elements	154278 / 560276
Cooling	Element order/sizing	Linear; default 31.397 mm
Cooling	Coolant setting	−70 °C
Cooling	Physical models	Energy on; laminar; radiation off

One mesh is used for each model. Adaptive sizing controls mesh generation, whereas convergence assessment requires comparison after successive refinement [8]. Structural indicators are maximum von Mises stress and total deformation. Thermal indicators are the contour color-scale range and local shelf temperature, with a shelf target of −40 °C.

1.5 Analytical Thickness Comparison

Strips of 10, 11, and 12 mm are compared against t_0 = 10 mm. At constant width, material, and local bending moment, $\sigma_b = M/W$ and mass per unit wall area $m_A = \rho t$ give Eq. (4), which quantifies the effects of section geometry.

$$I/I_0 = (t/t_0)^3; \quad W/W_0 = (t/t_0)^2;$$

$$\sigma_b/\sigma_{b0} = (t_0/t)^2; \quad m_A/m_{A0} = t/t_0 \quad (4)$$

2 RESULTS AND DISCUSSION

2.1 Stress and Deformation

Figure 4 reports a maximum von Mises stress of 288.1 MPa near the rear sidewall and rounded transition, with lower stresses at the front frame. Under the adopted criterion, $\eta = 1.0413$ and $n_y = 1.440$. The peak exceeds the benchmark by approximately 4.1%; reaching it would require a reduction of about 11.4 MPa, or 3.97% of the reported peak.

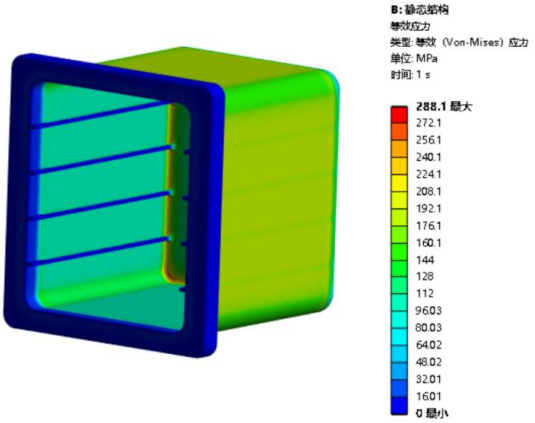


FIGURE 4: Static structural analysis: equivalent (von Mises) stress (MPa).

Figure 5 reports a maximum total deformation of 0.064835 mm near the rear edge, with smaller deformation at the front frame. The distributions identify the rear wall and transition as priorities for refinement; sealing suitability also depends on relative displacement at functional surfaces and assembly tolerances.

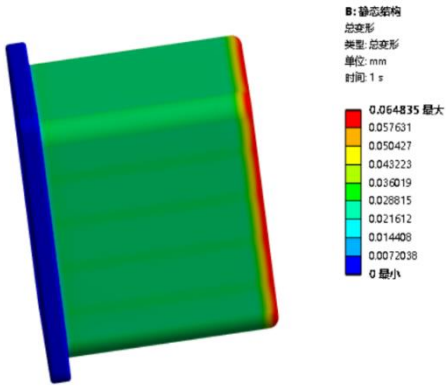


FIGURE 5: Static structural analysis: total deformation (mm).

2.2 Temperature Distribution

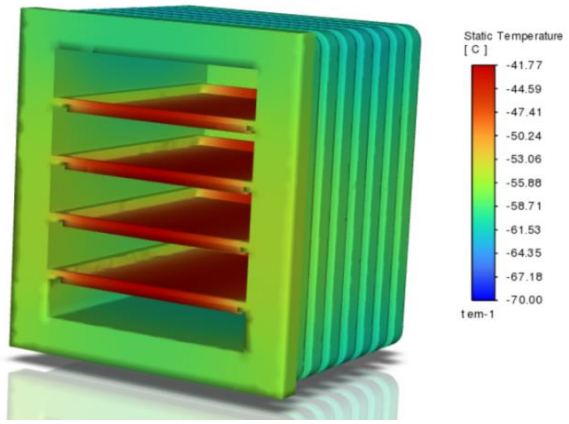


FIGURE 6: Overall temperature distribution in the chamber, channels, and shelves (°C).

Figure 6 spans −70.00 to −41.77 °C (28.23 °C). Channels and adjacent walls are colder; local shelf temperatures estimated from the contours are approximately −42 °C, about 2 °C below the −40 °C target. These estimates do not represent whole-shelf maximum or area-averaged temperatures.

Figure 7 spans −70.02 to −41.77 °C (28.25 °C), with shelves warmer than adjacent channels. The displayed lower endpoints differ by 0.02 °C. Color-scale spans do not measure within-shelf temperature variation, and these contours do not establish product freezing time.

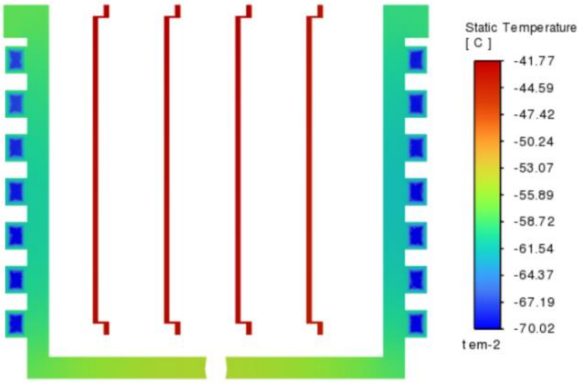


FIGURE 7: Sectional temperature distribution in the chamber and shelves (°C).

2.3 Wall Thickness and Mass

Table 2 compares local strips. At 11 and 12 mm, W increases by 21% and 44%, and I by 33.1% and 72.8%, relative to 10 mm. At constant bending moment, bending normal stress decreases by 17.4% and 30.6%, while mass per unit wall area increases by 10% and 20%.

TABLE 2: Analytical strip comparison (b = 1 mm; baseline t = 10 mm).

t (mm)	I (mm^4)	W (mm^3)	σ_b/σ_{b0}	m_A/m_{A0}
10	83.333	16.667	1.0000	1.00
11	110.917	20.167	0.8264	1.10
12	144.000	24.000	0.6944	1.20

Note: Bending moment, density, and wall area are held constant.

Thickening improves local bending resistance while increasing mass. Whole-chamber behavior also involves redistribution of internal forces, thermal stresses, and load paths. These ratios therefore cannot directly scale the 288.1 MPa von Mises peak or establish external-pressure stability of thicker designs.

2.4 Engineering Implications and Scope

Structural adjustments should prioritize the rear wall and rounded transition, considering thickness, corner radius, and support layout when comparing strength and mass. Thermal improvements should address heat transfer from channels to shelves. Coupled equipment- and vial-scale models can further relate chamber response to product behavior [5].

This study supports preliminary design assessment. Quantitative interpretation is limited by the completeness of boundary-condition descriptions, use of a single mesh, and contour-based temperature estimates. Supports, connections, temperature mapping, and cooling-flow boundaries affect model reproducibility. Mesh independence, heat balance, and experimental agreement are outside this assessment; further evaluation requires complete models, mesh refinement, and temperature measurements over usable shelf surfaces.

CONCLUSIONS

(1) For the 10 mm case, the reported maximum von Mises stress is 288.1 MPa, approximately 4.1% above the adopted 276.7 MPa benchmark; maximum total deformation is 0.064835 mm. This conditional comparison identifies the rear wall and rounded transition as priorities for refinement.

(2) At a constant local bending moment, 11 and 12 mm strips reduce bending normal stress by 17.4% and 30.6%, respectively, with mass per unit wall area increasing by 10% and 20%. These analytical ratios guide preliminary thickness selection, rather than establish whole-chamber performance.

(3) At a −70 °C coolant setting, local shelf temperatures estimated from the contours are approximately −42 °C. These readings support preliminary cooling assessment; shelf uniformity and product freezing require spatial statistics and time-dependent evaluation.

REFERENCES

[1] Carfagna, M., Rosa, M., Hawe, A., and Frieß, W. (2022). Design of freeze-drying cycles: The determination of heat transfer coefficient by using heat flux sensor and MicroFD. International Journal of Pharmaceutics, 621, 121763. doi: 10.1016/j.ijpharm.2022.121763

[2] [2] Piechnik, E., Smolka, J., Palacz, M., et al. (2024). Experimentally validated CFD-tool for a freezing simulation in a small-scale freeze-dryer. Journal of Food Engineering, 367, 111888. doi: 10.1016/j.jfoodeng.2023.111888

[3] Piechnik, E., Palacz, M., Tolstorebrov, I., et al. (2024). Design and evaluation of an R290-based freezing system and air distribution in a domestic-scale microwave-heated freeze-dryer prototype. Innovative Food Science & Emerging Technologies, 96, 103781. doi: 10.1016/j.ifset.2024.103781

[4] Srisuma, P., Barbastathis, G., and Braatz, R. D. (2024). Mechanistic modeling and analysis of thermal radiation in conventional, microwave-assisted, and hybrid freeze drying for biopharmaceutical manufacturing. International Journal of Heat and Mass Transfer, 221, 125023. doi: 10.1016/j.ijheatmasstransfer.2023.125023

[5] Zadravec, M., Metsi-Guckel, E., Kamenik, B., et al. (2025). Towards a digital twin of primary drying in lyophilization using coupled 3-D equipment CFD and 1-D vial-scale simulations. European Journal of Pharmaceutics and Biopharmaceutics, 208, 114662. doi: 10.1016/j.ejpb.2025.114662

[6] Kaiser Aluminum. (n.d.). Rod & Bar Alloy 2014: Technical Data (Rev. 05/06). (accessed October 26, 2026). Online source

[7] Roylance, D. (2000). Stresses in beams. Massachusetts Institute of Technology. (accessed October 25, 2026). Online source

[8] ANSYS, Inc. (2024). Using adaptive convergence. Mechanical User's Guide, Release 2024 R2. (accessed October 26, 2026). Online source